*Pre-Clinical Research Report*

*Journal of* INTERNATIONAL MEDICAL RESEARCH

Journal of International Medical Research
49(1) 1–16

DOI: 10.1177/0300060520986369
journals.sagepub.com/home/imr
SAGE

# Layer-specific strain for assessing the effect of naringin on systolic myocardial dysfunction induced by sepsis and its underlying mechanisms

**Li-juan Sun[1], Wei Qiao[2], Yang-jie Xiao[2] and Wei-dong Ren[2]**

## Abstract

**Objective:** This study aimed to investigate the protective effects of naringin on myocardial deformation and oxidative responses in rats with sepsis-induced myocardial dysfunction (SIMD).

**Methods:** Global and segmental layer-specific longitudinal strain (LS) was assessed by speckle tracking echocardiography. Serum levels of creatine kinase, lactate dehydrogenase, superoxide dismutase, and malondialdehyde were measured. The activity of cleaved caspase-3 was determined by immunohistochemistry. Protein expression levels of Kelch-like ECH-related protein 1 (Keap1), nuclear erythroid factor 2-related factor 2 (Nrf2), and heme oxygenase-1 (HO-1) were measured by western blotting.

**Results:** Naringin inhibited the lipopolysaccharide-induced decrease in global and layer-specific LS of the left ventricle. Naringin also increased superoxide dismutase expression and decreased malondialdehyde, creatine kinase, lactate dehydrogenase, and cleaved caspase-3 expression in rats with SIMD. Furthermore, naringin increased Nrf2 and HO-1 protein expression levels, and decreased Keap1 protein expression levels in rats with SIMD.

**Conclusion:** Layer-specific LS analysis of myocardial function by speckle tracking echocardiography can reflect early changes in myocardial systolic function. Naringin may possess a protective effect through moderating lipopolysaccharide-induced myocardial oxidative stress via the Keap1/Nrf2/HO-1 pathway in rats with SIMD.

[1]Department of Ultrasound, First Hospital of Qinhuangdao, Qinhuangdao, P.R. China
[2]Department of Ultrasound, Shengjing Hospital of China Medical University, Shenyang, P.R. China

**Corresponding author:**
Li-juan Sun, First Hospital of Qinhuangdao, 258 Wenhua St, Haigang District, Qinhuangdao 066000, Hebei, China.
Email: sunlj819@163.com

**Keywords**
Septic cardiomyopathy, naringin, longitudinal strain, myocardial layer, oxidative stress, speckle tracking echocardiography

Date received: 30 September 2020; accepted: 8 December 2020

## Introduction

Sepsis is a life-threatening organ dysfunction syndrome caused by susceptibility of the host to severe infections.[1] Septic shock and multiorgan failure caused by sepsis are the leading cause of death and critical illness worldwide in the adult intensive care unit.[2] Sepsis-induced myocardial dysfunction (SIMD), caused by bacterial endotoxin lipopolysaccharide (LPS), directly increases mortality of patients with sepsis.[3] Therefore, reducing myocardial dysfunction of sepsis in patients is critical for prolonging life and preventing morbidity.

Several mechanisms of SIMD have been hypothesized, but excessive production of proinflammatory factors and cytotoxic free radicals are the most widely accepted mechanisms. After LPS stimulation, myocardial cells can produce reactive oxygen species, which elicit the oxidative stress response, impairing mitochondrial function.[4] Additionally, LPS can stimulate immune cells and this produces a variety of pro-inflammatory factors.[5] Moreover, overexpression of nitric oxide can affect cardiac L-type calcium channels, inhibit mitochondrial function, and induce apoptosis of cardiac myocytes.[6] Therefore, inhibition of oxidative stress may be an effective treatment for LPS-induced cardiac injury. Heme oxygenase-1 (HO-1) is a heat shock protein that can be induced by a variety of substances or stimulants. HO-1 also has a protective effect on the cardiovascular system.[7] Induction of HO-1 is related to activation of the transcription factor nuclear erythroid factor 2 (NE-F2)-related factor 2 (Nrf2).[8] Under normal circumstances, Nrf2 binds to Kelch-like ECH-related protein 1 (Keap1) in the cytoplasm. When intracellular redox imbalance occurs, free Nrf2 binds to antioxidant response elements in the nucleus. Activation of Nrf2 regulates the biological activity of many phase II detoxification enzymes, such as HO-1. Previous studies have also suggested that activation of the Nrf2/HO-1 pathway attenuates hypoxia-stimulated H9c2 cell apoptosis.[9]

Naringin is a natural flavonoid compound found in grapefruit and related citrus plants. Naringin possesses natural antioxidant, anti-inflammatory, anti-apoptotic, and cardiovascular protective effects.[10–12] Naringin regulates oxidative stress-induced apoptosis and the inflammatory response through intrinsic and extrinsic pathways, thereby effectively protecting pancreatic $\beta$-cells in insulin-deficient diabetic mice.[13] Naringin also ameliorates arsenic-induced cardiotoxicity, which is related to the Nrf2/HO-1 pathway.[14] Previously, we reported the effect of naringin on the inflammatory response of SIMD and its molecular mechanism.[15]

Speckle-tracking echocardiography (STE) is an angle-independent ultrasound technique for evaluating global and segmental deformation of the myocardium. A recent development in layer-specific STE analysis allows quantitative analysis of deformation of the myocardium's three layers, including the endocardium,

myocardium, and epicardium. This new sensitive indicator is effective for detecting cardiac dysfunction in various heart diseases, and it may be sensitive enough to detect subtle abnormalities in cardiac function over and above global strain.[16–18] We previously reported changes in global layer-specific strain of the left ventricle (LV) in rats with SIMD, followed by the therapeutic effect of naringin.[15] In this study, we aimed to investigate the protective effects of naringin on myocardial deformation and oxidative responses in rats with SIMD.

## Methods

### Experimental animals

The experimental protocol was approved by the Ethics Committee of Shengjing Hospital of China Medical University (No: 2018PS05K). Adult male Sprague–Dawley rats (HFK Bioscience Co., Beijing, China) aged 8 to 9 weeks and weighing 295 to 305 g were bred in a pathogen-free laboratory (Certificate No: SYXK [Liao] 2017-0004). Rats were housed at 22°C to 24°C with 70% humidity. Rats were kept in a 12-hour/12-hour light/dark cycle for at least 7 days.

### Rat models and treatment protocols

Rats were randomly divided into four groups as follows (n = 15 in each group). In the control group, rats were administered physiological saline (same volume as naringin) by oral gavage for 7 days. Approximately 1 hour after the last administration on day 7, rats were intraperitoneally injected with physiological saline (same volume as LPS). In the LPS group, rats were administered with physiological saline (same volume as naringin) by oral gavage for 7 days. Approximately 1 hour after the last administration on day 7, rats were intraperitoneally injected with LPS (*Escherichia coli* O111: B4; Sigma-Aldrich, St. Louis, MO, USA) at a dose of 10 mg/kg.[19] Naringin treatment groups included the LPS + naringin 50 mg/kg/day ($Nar_{50}$) group and the LPS + naringin 100 mg/kg/day ($Nar_{100}$) group. Rats were administered with naringin (Sigma-Aldrich) by oral gavage at a dose of 50 or 100 mg/kg/day for 7 days.[20,21] Approximately 1 hour after the last administration on day 7, rats were intraperitoneally injected with LPS (10 mg/kg). Six hours after administration of LPS,[22] the rats were anesthetized, and then the following operations were performed (Figure 1).

### Conventional echocardiography

For evaluation of echocardiography, we used a GE Vivid E9 ultrasound machine (GE Healthcare, Horten, Norway), which was equipped with a 12S transducer with a frequency of 9 to 12 MHz. The following echocardiographic parameters were measured in each group: left ventricular end-diastolic diameter (LVEDd), left ventricular end-systolic diameter (LVEDs), left ventricular ejection fraction (LVEF), peak early diastolic velocity (E) of mitral inflow, early diastolic velocity at the septal side of the mitral annulus (E′), and the E/E′ ratio. These parameters were measured three times by conventional ultrasound and tissue Doppler imaging, and then an average value was taken.

### Global and segmental layer-specific longitudinal strain analysis

We acquired five consecutive cardiac cycles of the LV long axis three-chamber view, the apical four-chamber view, and the apical two-chamber view. STE quantitative analysis was performed on an offline software station (EchoPAC V201; GE Healthcare, Horten, Norway). The clearest image of the endocardium was selected and the

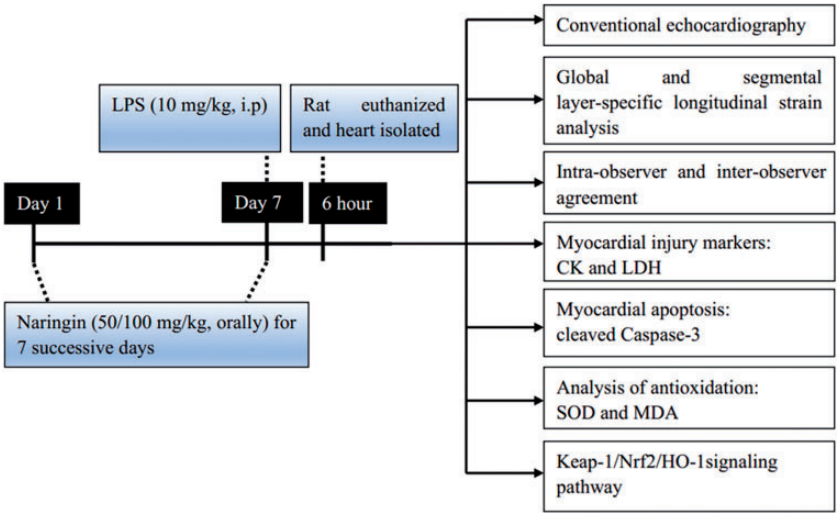


**Figure 1.** Schematic diagram of the experimental procedures.
LPS, lipopolysaccharide; CK, creatine kinase; LDH, lactate dehydrogenase, SOD, superoxide dismutase; MDA, malondialdehyde; Keap1, Kelch-like ECH-related protein 1; Nrf2; nuclear erythroid factor 2-related factor 2; HO-1, heme oxygenase-1.

endocardial contour was manually outlined. The region of interest was adjusted to match the outline of the endocardium. The LV wall was automatically divided into three myocardial layers by the analysis software, which was used to assess the longitudinal strain (LS) of the endocardial layer, the mid-myocardial layer, and the epicardial layer. The LV was divided into 18 myocardial segments, which included six segments (anteroseptal, anterior, lateral, inferior, posterior, and septal) at the basal, mid-ventricular, and apical levels. The peak systolic LS of the three layers of the myocardium were obtained from the three apical views. The global longitudinal strain (GLS) was obtained from the mean values of myocardial deformation at three levels involving the endocardial layer (GLS-endo), mid-myocardial layer (GLS-mid), and epicardial layer (GLS-epi). The mean value of all myocardial segments was represented as ventricular GLS. The transmural gradient was the absolute value of the difference between GLS-endo and GLS-epi.

### *Intra-observer and inter-observer agreement*

Twenty rats were randomly selected and re-measured by two experienced ultrasound physicians who were blinded to the grouping of the rats. Intra-observer reproducibility of GLS-endo, GLS-mid, and GLS-epi was performed by the same ultrasound physician using off-line data at different time points. Inter-observer reproducibility of these parameters was performed by two ultrasound physicians who repeated measurements from the same images.

### *Estimation of myocardial injury markers*

After ultrasonic examination under anesthesia, the chest of the rats was opened to expose the heart. Blood was drawn from the right ventricle into a heparin-coated tube,

and plasma was obtained by centrifuging the blood at 1370 × g for 10 minutes at room temperature. Serum levels of creatine kinase (CK) and lactate dehydrogenase (LDH) were determined using an automatic biochemical analyzer (IDEXX Laboratories Inc., Westbrook, ME, USA).

### Immunohistochemistry

Myocardial tissues were prepared into 4-μm sections, then deparaffinized and boiled in citric acid buffer (pH 6.0) for antigen retrieval. Primary antibody against cleaved caspase-3 (1:200 dilution; Wanleibio, Shenyang, China) was applied at 4°C overnight. Secondary antibody was applied at room temperature for 25 minutes. After fully dipping sections in phosphate-buffered saline, horseradish enzyme-labeled streptavidin was added for 30 minutes. Finally, 3,3′-diaminobenzidine was used as a chromogen, and hematoxylin was used for counterstaining. Caspase-3 expression was scored by the staining intensity (negative, mild, moderate, or high) and the positive percentage in heart tissue sections as previously described.[15]

### Analysis of antioxidation

The activity of superoxide dismutase (SOD) in rat serum was determined by the xanthine oxidase method according to the manufacturer's instructions (Jiancheng, Nanjing, China). Serum samples were taken from a −20°C freezer and thawed on ice. According to the instructions, the reagents were prepared and added to a 96-well plate, mixed, and incubated at 37°C for 20 minutes. After the reaction, the optical density value was measured at 450 nm. An activity unit of SOD was the corresponding enzyme amount when the SOD inhibition rate reached 50%.

Malondialdehyde (MDA) content in rat serum was determined by the thiobarbituric acid method. The reagents were added to centrifuge tubes according to the manufacturer's instructions (Jiancheng), mixed, and bathed in 95°C water for 40 minutes. The tubes were taken out and cooled with flowing water, and then centrifuged at 1370 × g for 10 minutes. The supernatant of each tube was collected and the absorbance value was measured at 532 nm.

### Western blot analysis

Myocardial tissue stored at −80°C was lysed and homogenized in ice-cold radioimmune precipitation lysis buffer, which was supplemented with 1% v/v phenylmethyl sulfonyl fluoride (Beyotime, Shanghai, China). Nuclear protein component was extracted according to the manufacturer's instructions (Invents, Biotechnologies, Beijing, China). The tissue homogenate was centrifuged at 14,000 × g for 20 minutes at 4°C. Equal amounts of denatured proteins were electrophoresed on sodium dodecyl sulfate-polyacrylamide gel electrophoresis and then transferred to polyvinylidenefluoride membranes (Millipore, Bedford, MA, USA). After blocking with 5% skimmed milk for 2 hours at room temperature, the membranes were then incubated with primary antibodies against Keap1 (1:1000 dilution; Abcam, San Diego, CA, USA), Nrf2 (1:500 dilution; Abcam), HO-1 (1:500 dilution; Abcam), Lamin B (1:1000 dilution; Wanleibio, Shenyang, China), and $\beta$-actin (1:10,000 dilution; Proteintech, Chicago, IL, USA) at 4°C overnight and incubated with a secondary antibody (1:20,000 dilution; Proteintech) coupled with horseradish peroxidase. Membranes were finally visualized using an enhanced chemiluminescence kit (GE Healthcare Life Sciences, Pittsburgh, PA, USA).

### Statistical analysis

Values are presented as mean ± standard deviation. For all analyses, IBM SPSS 19.0 software (IBM Corp., Armonk, NY, USA) was used. Comparison of data among the four groups was performed by one-way ANOVA. Reproducibility was assessed by Bland–Altman analysis. The level of significance was set at $P < 0.05$.

## Results

### Detection of LV deformation by conventional echocardiography in rats with SIMD

Four (6.67%) rats were excluded owing to a poor echo window, including one in the control group, one in the LPS group, and two in the LPS + $Nar_{100}$ group. Finally, 56 rats underwent echocardiographic analysis. Table 1 shows comparison of conventional echocardiographic parameters among the four groups of rats. There were no significant differences in body weight, heart rate, and E of mitral inflow among the four groups. LVEF and LVEDs were not significantly different in the LPS + $Nar_{50}$ group compared with the LPS group. LVEF and E′ were significantly lower in the LPS group compared with the control group (both $P < 0.01$). LVEDd, LVEDs, and the E/E′ ratio were significantly higher in the LPS group compared with the control group (all $P < 0.05$), and these were significantly attenuated by naringin administration, especially in the LPS + $Nar_{100}$ group (all $P < 0.05$).

### Changes in layer-specific LS in rats with SIMD

GLS in all three layers and the transmural LS gradient were significantly lower in the LPS group compared with the control group (all $P < 0.01$). GLS in all three layers and the transmural LS gradient were significantly attenuated by naringin administration, except for GLS-epi in the LPS + $Nar_{50}$ group (Table 1, Figure 2).

Layer-specific LS myocardial deformation parameters at three ventricular levels were evaluated (Table 2). Peak systolic LS-endo, LS-mid, and LS-epi at the LV basal, mid-ventricular, and apical levels were significantly lower in the LPS group compared with the control group (all $P < 0.05$). These values recovered after naringin administration, especially in the LPS + $Nar_{100}$ group (all $P < 0.05$ in the LPS + $Nar_{100}$ group vs the LPS group). Myocardial strain was highest in the endocardial layer, and gradually decreased from the endocardial layer to the epicardial layer. As shown in Figure 3, peak systolic LS-endo, LS-mid, and LS-epi in the four groups gradually increased from the basal to the apical levels (all $P < 0.05$), with the highest values in the apical level and the lowest in the basal level.

The consistency limits of GLS-endo, GLS-mid, and GLS-epi for the intra-observer measurements were −3.92 to 4.50, −2.83 to 3.37, and −1.82 to 2.29, respectively, and those for the inter-observer measurements were −5.04 to 5.64, −5.49 to 5.16, and −3.69 to 4.29, respectively (Figure 4).

### Naringin alleviates myocardial apoptosis in rats with SIMD

Expression of cleaved caspase-3 activity was significantly higher in the LPS group compared with the control group ($P < 0.01$, Figure 5). As expected, pretreatment with naringin inhibited the activity of cleaved caspase-3 in a dose-dependent manner (both $P < 0.01$). These results suggest a role of naringin in attenuating myocardial apoptosis in rats with SIMD.

**Table 1.** Comparison of echocardiographic parameters in rats with sepsis-induced myocardial dysfunction.

| Variable | Control group (n = 14) | LPS group (n = 14) | LPS+$N_{50}$ group (n = 15) | LPS+$N_{100}$ group (n = 13) |
|---|---|---|---|---|
| Weight (g) | 298.75 ± 4.47 | 297.96 ± 4.62 | 299.20 ± 4.91 | 298.60 ± 4.17 |
| HR (bpm) | 445.86 ± 40.56 | 466.71 ± 41.33 | 456.00 ± 39.61 | 453.38 ± 45.71 |
| LVEDd (mm) | 5.46 ± 0.50 | 6.14 ± 0.85$^{*}$ | 5.63 ± 0.70$^{\#}$ | 5.26 ± 0.56$^{\#\#}$ |
| LVEDs (mm) | 2.75 ± 0.40 | 3.63 ± 0.36$^{**}$ | 3.40 ± 0.34 | 3.03 ± 0.29$^{\#\#}$ |
| E (m/s) | 0.85 ± 0.06 | 0.89 ± 0.07 | 0.87 ± 0.06 | 0.91± 0.06 |
| E' (m/s) | 0.09 ± 0.01 | 0.06 ± 0.01$^{**}$ | 0.08 ± 0.01$^{\#\#}$ | 0.09 ± 0.01$^{\#\#\triangle}$ |
| E/E' | 9.89 ± 1.01 | 15.35 ± 2.12$^{**}$ | 10.82 ± 1.63$^{\#\#}$ | 10.13 ± 0.69$^{\#\#}$ |
| LVEF (%) | 78.63 ± 8.44 | 66.62 ± 8.15$^{**}$ | 69.82 ± 7.85 | 77.96 ± 8.04$^{\#\#\triangle}$ |
| GLS-endo (%) | −24.62 ± 5.25 | −16.18 ± 6.15$^{**}$ | −21.51 ± 3.25$^{\#}$ | −23.56 ± 6.28$^{\#\#}$ |
| GLS-mid (%) | −20.30 ± 5.18 | −13.64 ± 5.05$^{**}$ | −18.27 ± 5.07$^{\#}$ | −19.92 ± 5.78$^{\#\#}$ |
| GLS-epi (%) | −15.07 ± 3.37 | −10.89 ± 3.65$^{**}$ | −12.80 ± 2.58 | −15.04 ± 3.29$^{\#\#}$ |
| GLS (%) | −20.00 ± 2.38 | −13.57 ± 2.99$^{**}$ | −17.53 ± 2.62$^{\#\#}$ | −19.51 ± 3.79$^{\#\#}$ |
| Transmural gradient (%) | 9.55 ± 2.13 | 5.65 ± 2.20$^{**}$ | 8.70 ± 1.07$^{\#}$ | 9.63 ± 5.34$^{\#\#}$ |

Values are presented as mean ± standard deviation. $^{*}P < 0.05$, $^{**}P < 0.01$ vs. the control group; $^{\#}P < 0.05$, $^{\#\#}P < 0.01$ vs. the LPS group; $^{\triangle}P < 0.05$ vs. the LPS + $Nar_{50}$ group.

LPS, lipopolysaccharide; $Nar_{50}$, naringin 50 mg/kg/day; $Nar_{100}$, naringin 100 mg/kg/day; HR, heart rate; bpm, beats per minute; LVEDd, left ventricular end-diastolic diameter; LVEDs, left ventricular end-systolic diameter; E, peak early diastolic velocity; E′, early diastolic velocity at the septal side of the mitral annulus; LVEF, left ventricular ejection fraction; GLS-endo, global longitudinal strain in the endocardial layer; GLS-mid, global longitudinal strain in the mid-myocardial layer; GLS-epi, global longitudinal strain in the epicardial layer.

### *Naringin increases SOD activity and decreases MDA, and CK and LDH levels in rats with SIMD*

As myocardial marker enzymes, the myocardial injury parameters CK and LDH are usually used to measure the severity of ischemic heart disease. Expression of CK (Figure 6a) and LDH (Figure 6b) was significantly higher in the LPS group compared with the control group (both $P < 0.01$). However, naringin pretreatment dramatically reduced CK and LDH levels compared with LPD treatment (both $P < 0.01$). The activity of SOD (Figure 6c) and MDA (Figure 6d) in serum was examined to verify the antioxidant activity of naringin. SOD activity was significantly lower and the content of MDA in serum was lower in the LPS group compared with the control group (both $P < 0.01$). Pretreatment with naringin reversed the changes in MDA content and SOD activity by LPS in a dose-dependent manner (all $P < 0.01$).

### *Effects of naringin on Keap1/Nrf2/HO-1 expression in rats with SIMD*

To estimate naringin's capability to activate Nrf2 signaling in myocardial tissues, Keap1, Nrf2, and HO-1 protein levels were assessed (Figure 7). Challenge with LPS increased Keap1, Nrf2, and HO-1 protein levels (all $P < 0.01$ vs controls). Nrf2 and HO-1 protein levels were significantly higher, and Keap1 protein levels were significantly lower in the naringin + LPS groups compared with the LPS group (all $P < 0.05$).

## Discussion

Oxidative stress is a risk factor for myocardial dysfunction caused by sepsis.[19] Naringin is a flavonoid glycoside that has

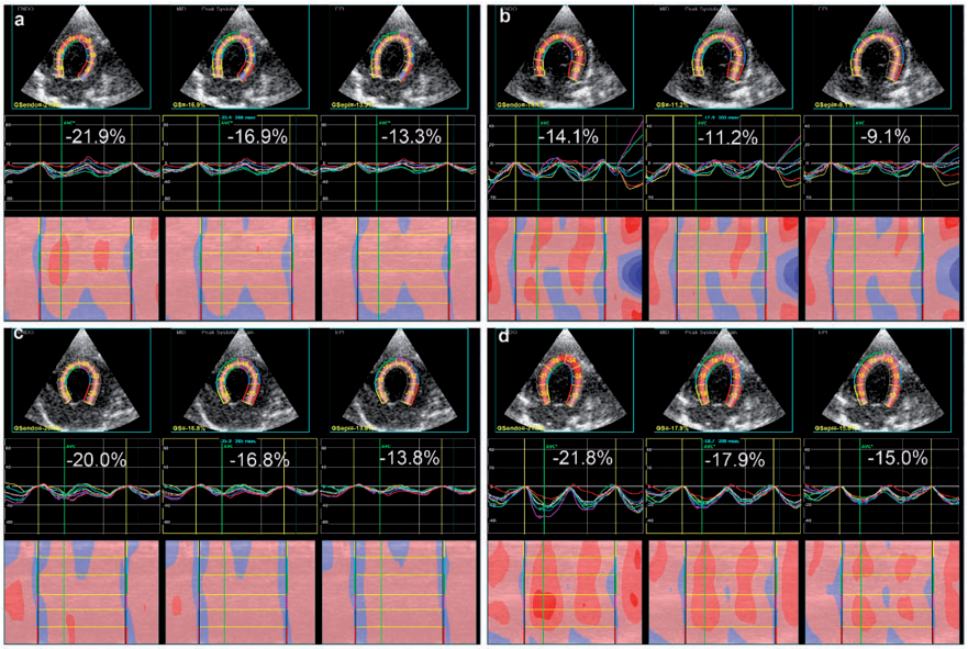


**Figure 2.** Longitudinal layered strain in the control (a), LPS (b), LPS + $Nar_{50}$ (c), and LPS + $Nar_{100}$ (d) groups. Endocardial, mid-myocardial, and epicardial strain is arranged from left to right in each graph. The related strain curves for the six segments within the longitudinal-axis view are shown. Color lines indicate regional strain and white dotted lines indicate the global (average) strain.
LPS, lipopolysaccharide; $Nar_{50}$, naringin 50 mg/kg/day; $Nar_{100}$, naringin 100 mg/kg/day; LS-endo, longitudinal strain of the endocardial layer; LS-mid, longitudinal strain of the mid-myocardial layer; LS-epi, longitudinal strain of the epicardial layer.

**Table 2.** Effects of naringin on left ventricular three-layer longitudinal strain at the basal, mid-ventricular, and apical levels in rats with sepsis-induced myocardial dysfunction.

| LS (%) | Control group (n = 14) | LPS group (n = 14) | LPS+$N_{50}$ group (n = 15) | LPS+$N_{100}$ group (n = 13) |
|---|---|---|---|---|
| Basal level | | | | |
| LS-endo | −17.49 ± 3.86 | −11.57 ± 4.28$^{**}$ | −15.13 ± 3.41$^{\#}$ | −16.23 ± 4.61$^{\#\#}$ |
| LS-mid | −15.95 ± 3.77 | −9.93 ± 3.85$^{**}$ | −12.09 ± 4.11 | −13.51 ± 4.96$^{\#}$ |
| LS-epi | −12.45 ± 3.26 | −8.59 ± 2.71$^{**}$ | −10.00 ± 2.47 | −12.38 ± 2.86$^{\#\#}$ |
| Mid-ventricular level | | | | |
| LS-endo | −23.15 ± 5.74 | −14.77 ± 6.34$^{**}$ | −20.01 ± 4.18$^{\#}$ | −21.81 ± 6.99$^{\#\#}$ |
| LS-mid | −19.77 ± 6.73 | −13.46 ± 7.09$^{*}$ | −19.20 ± 5.46$^{\#}$ | −20.73 ± 8.55$^{\#\#}$ |
| LS-epi | −14.49 ± 3.75 | −10.93 ± 3.88$^{*}$ | −10.82 ± 2.53 | −14.25 ± 4.32$^{\#\triangle}$ |
| Apical level | | | | |
| LS-endo | −33.22 ± 7.32 | −23.62 ± 9.50$^{**}$ | −29.37 ± 5.62$^{\#}$ | −32.63 ± 7.89$^{\#\#}$ |
| LS-mid | −25.17 ± 7.45 | −17.52 ± 6.63$^{**}$ | −23.53 ± 8.27$^{\#}$ | −25.54 ± 6.42$^{\#\#}$ |
| LS-epi | −18.27 ± 5.69 | −13.16 ± 5.43$^{*}$ | −17.59 ± 5.93$^{\#}$ | −18.48 ± 5.39$^{\#}$ |

Values are presented as mean ± standard deviation. $^{*}P < 0.05$, $^{**}P < 0.01$ vs. the control group; $^{\#}P < 0.05$, $^{\#\#}P < 0.01$ vs. the LPS group; $^{\triangle}P < 0.05$ vs. the LPS + $Nar_{50}$ group.
LPS, lipopolysaccharide; $Nar_{50}$, naringin 50 mg/kg/day; $Nar_{100}$, naringin 100 mg/kg/day; LS-endo, longitudinal strain in the endocardial layer; LS-mid, longitudinal strain in the mid-myocardial layer; LS-epi, longitudinal strain in the epicardial layer.

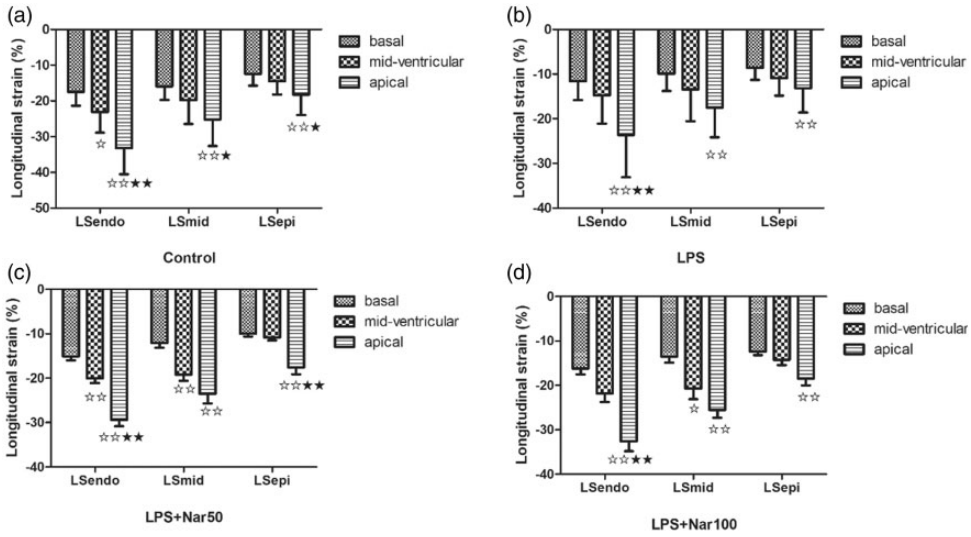


**Figure 3.** Longitudinal layered strain of the left ventricle at the basal, mid-ventricular, and apical levels in the control group (a), LPS group (b), LPS + $Nar_{50}$ group (c), and LPS + $Nar_{100}$ group (d). Values are presented as mean ± standard deviation. ☆$P < 0.05$, ☆☆$P < 0.01$ vs. the basal level; ★$P < 0.05$, ★★$P < 0.01$ vs. the mid-ventricular level.
LPS, lipopolysaccharide; $Nar_{50}$, naringin 50 mg/kg/day; $Nar_{100}$, naringin 100 mg/kg/day.

many pharmacological and therapeutic effects.[23] However, there have been no reports on the molecular mechanism of naringin's protective effect on oxidative stress damage and LV segmental layer-specific LS in rats with SIMD. To the best of our knowledge, this study is the first to show the mechanism of naringin's effect on oxidative stress damage in rats with SIMD.

Real-time tracking of the location of different pixels within myocardial tissues in two-dimensional images was reviewed by STE analysis in our study. STE quantitatively analyzes speckle echoes to provide information about the global and segmental function of the LV. A previous study showed that STE parameters were more sensitive than traditional methods when evaluating LPS-induced myocardial dysfunction in mice.[24] We found that the three layers of peak systolic GLS and conventional LV functional characteristics in the LPS group were lower than those in the control group. In fact, the greatest decrease in GLS occurred in the endocardial layer. GLS in the naringin treatment groups was higher than that in the LPS group, but improvement of conventional LV functional characteristics was not obvious in the low dose naringin group. This finding indicated that longitudinal movement injury of the myocardium in rats treated with LPS was alleviated by naringin. Therefore, naringin improved LV systolic dysfunction in rats with SIMD. Conventional echocardiography showed decreased diastolic function in the LPS group (E′ was decreased and E/E′ was increased), which was significantly attenuated by naringin administration. However, LVEF and LVEDs were not significantly different in the LPS + $Nar_{50}$ group compared with the LPS group. STE is more sensitive than conventional echocardiography in evaluating the efficacy of naringin.

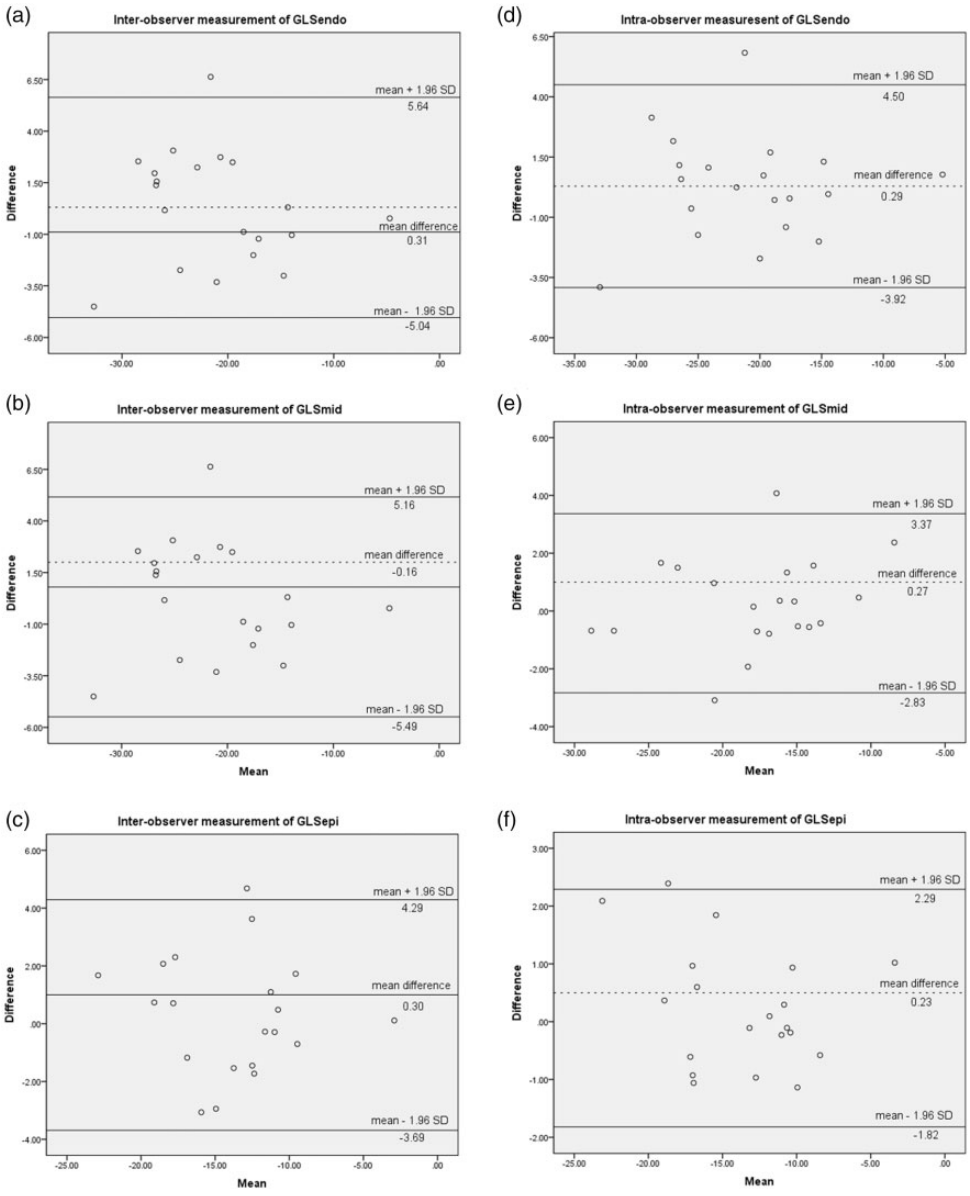


**Figure 4.** Bland–Altman analyses of GLS-endo, GLS-mid, and GLS-epi for inter-observer (a), (b), and (c) and intra-observer (d), (e), and (f) measurements, respectively.
GLS-endo, global longitudinal strain of the endocardial layer; GLS-mid, global longitudinal strain of the mid-myocardial layer; GLS-epi, global longitudinal strain of the epicardial layer.

Recently, STE has become able to automatically grade each segment according to the speckle tracking quality. This is achieved by dividing the LV wall thickness into the endocardial layer, mid-myocardial layer, and epicardial layer, so that the three layers can be quantified separately.[25] Layer-specific quantification of myocardial

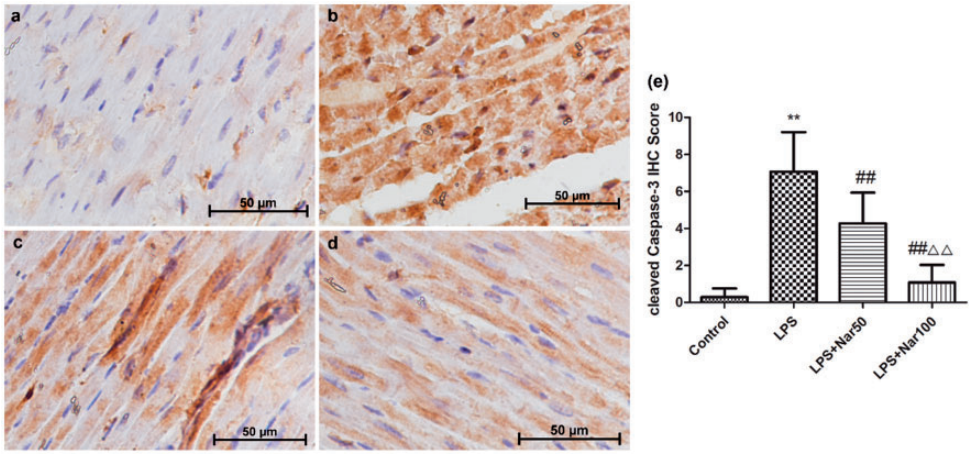


**Figure 5.** Immunohistochemistry shows that cleaved caspase-3 levels are decreased in rats with sepsis-induced myocardial dysfunction treated with naringin (light microscopy, hematoxylin and eosin stain, × 400). Control group (a), LPS group (b), LPS + $Nar_{50}$ group (c), LPS + $Nar_{100}$ group (d), and immunohistochemical scores of cleaved caspase-3 (e). Values are presented as mean ± standard deviation. $^{**}P < 0.01$ vs. the control group; $^{\#\#}P < 0.01$ vs. the LPS group; $^{\triangle\triangle}P < 0.01$ vs. the LPS + $Nar_{50}$ group.
LPS, lipopolysaccharide; $Nar_{50}$, naringin 50 mg/kg/day; $Nar_{100}$, naringin 100 mg/kg/day.

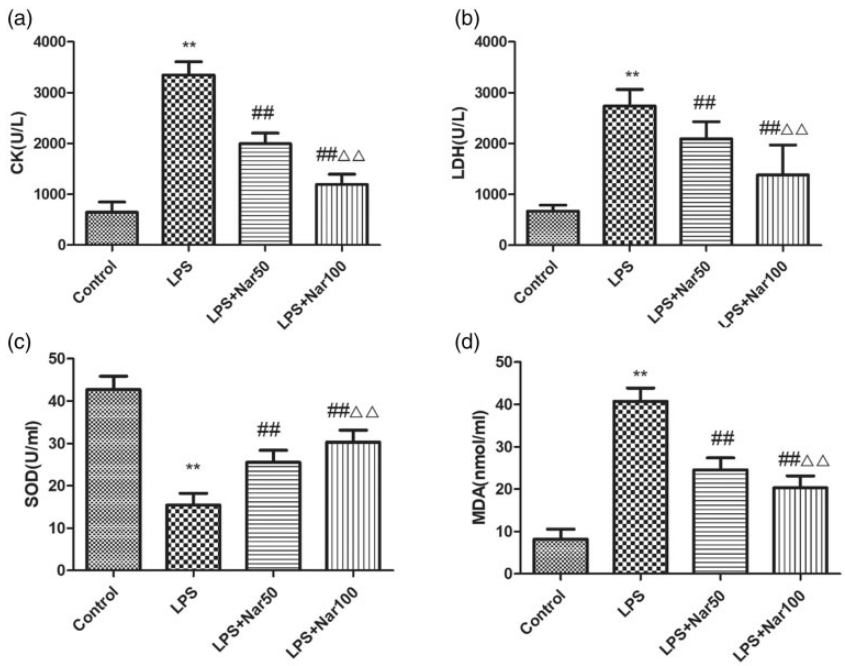


**Figure 6.** Effects of naringin on CK (a), LDH (b), SOD (c), and MDA (d) in rats with sepsis-induced myocardial dysfunction. Values are presented as mean ± standard deviation. $^{**}P < 0.01$ vs. the control group; $^{\#\#}P < 0.01$ vs. the LPS group; $^{\triangle\triangle}P < 0.01$ vs. the LPS + $Nar_{50}$ group.
CK, creatine kinase; LDH, lactate dehydrogenase, SOD, superoxide dismutase; MDA, malondialdehyde; LPS, lipopolysaccharide; $Nar_{50}$, naringin 50 mg/kg/day; $Nar_{100}$, naringin 100 mg/kg/day.

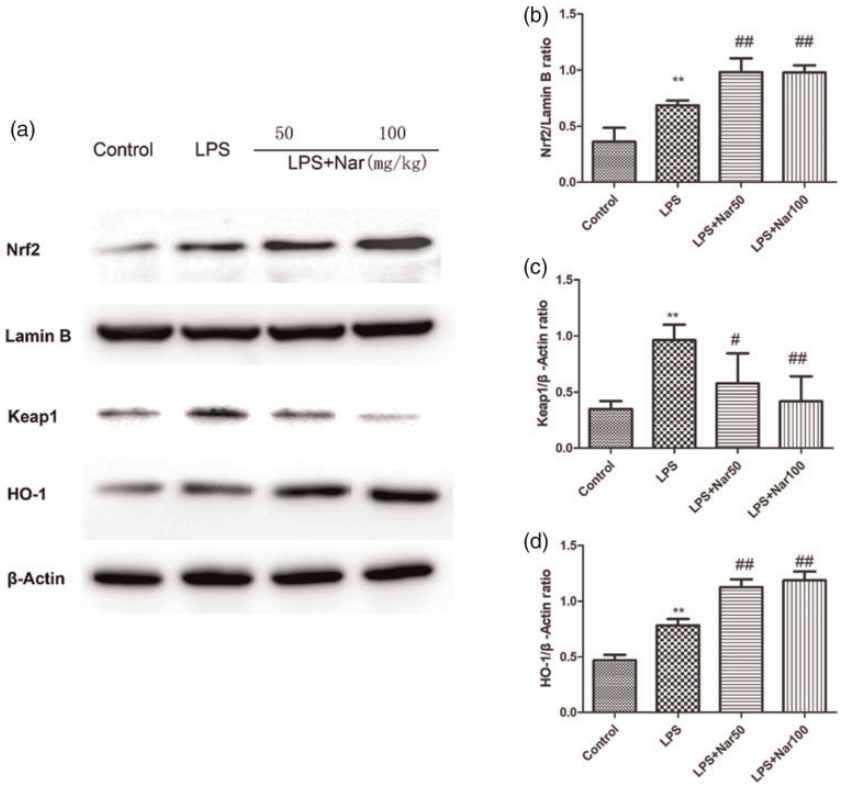


**Figure 7.** Effects of naringin on Nrf2 (a, b), Keap1 (a, c), and HO-1 (a, d) expression in rats with sepsis-induced myocardial dysfunction. Values are presented as mean ± standard deviation. $^{**}P < 0.01$ vs. the control group; $^{\#\#}P < 0.01$ vs. the LPS group.
Nrf2, nuclear erythroid 2-related factor 2; Keap1, Kelch-like ECH-related protein 1; HO-1, heme oxygenase-1; LPS, lipopolysaccharide; $Nar_{50}$, naringin 50 mg/kg/day; $Nar_{100}$, naringin 100 mg/kg/day.

function has been investigated in many cardiovascular diseases.[25,26] However, previous studies on LV strain of SIMD mainly focused on global strain, without further analysis of myocardial damage in different layers of the LV. Layer-specific STE might have higher sensitivity than global strain for detecting subtle myocardial functional abnormalities.[17,18] In the current study, multilayer strain in all three layers and a transmural LS gradient were significantly decreased after LPS administration. Moreover, myocardial strain was highest in the endocardial layer, and gradually decreased from the endocardial layer to the epicardial layer. Potential causes for these findings might be as follows: 1) increased stress of the end-diastolic wall on the subendocardial myocardium, 2) differences in coronary artery perfusion and metabolism between the subendocardial and subepicardial myocardium, and 3) the subendocardial myocardium has a large motion range and consumes a lot energy.[27,28] Myocardial strain at the three levels of the LV was lowest at the base, which increased gradually from the base to the apex. The LV myocardium moves toward the bottom of the heart during systole. Therefore, the role of ventricular systolic activity increases gradually from the base to the apex of the myocardium.

We found that treatment with naringin resulted in a significant increase in LV strain parameters. Careful assessment of the endocardial layer might improve the accuracy of diagnosing SIMD and the efficacy of naringin.

Oxidative stress plays a crucial role in cardiovascular disease and cardiac dysfunction.[29] The imbalance between oxidation and antioxidant factors in the heart's defense system is caused by excessive production of free radicals and consumption of antioxidants.[30] SOD is an important myocardial antioxidant enzyme that scavenges oxygen free radicals.[31] MDA is a common biomarker of lipid peroxidation and an indirect marker of cellular oxidative damage.[32] An abnormal increase in MDA and reduction in SOD may be an important factor leading to myocardial injury caused by superoxide anion accumulation.[33] In this study, we found that naringin reduced MDA levels and increased SOD levels in rats with SIMD. This observation suggested that naringin played a certain protective role in LPS-induced cardiac injury by decreasing the release of oxidative mediators. After naringin pretreatment, the effect of LPS on serum CK and LDH levels in rats was also significantly reduced. Apoptosis is a programmed cell death that is critical for tissue development and homeostasis. Caspase-3 is the main mediator of apoptosis and necrosis. In our study, pretreatment with naringin inhibited the activity of cleaved caspase-3 in a dose-dependent manner. These results indicate that naringin has a certain protective effect on LPS-induced myocardial injury.

Nrf2, as a redox-sensitive transcription factor, plays a major role in redox homeostasis and interacts with many protective factors.[34] Nrf2 is activated after release from Keap1 in the presence of oxidative stress. Activation of Nrf2 can regulate the expression of the downstream molecule HO-1, which has detoxification and antioxidant properties. As an endogenous antioxidant, HO-1 reduces oxidative stress and degrades heme into carbon monoxide, biliverdin, and ferrous iron, thereby protecting cells and tissues from oxidative stress.[35] Previous studies have shown that naringin inhibits arsenite-induced cardiotoxicity by regulating the transforming growth factor-$\beta$/Smad-3 and Nrf2/HO-1 pathways.[14] In LPS-induced acute lung injury in mice, inhibition of oxidative stress was largely dependent on the Keap1/Nrf2 signaling pathway.[36] In the present study, protein expression levels of Keap1, Nrf2, and HO-1 were significantly higher in the LPS group compared with the control group. However, pretreatment with naringin significantly increased the expression of Nrf2 and HO-1, and decreased that of Keap1 in rats with SIMD. These results suggest that naringin is related to the Keap1/Nrf2/HO-1 signaling pathway in reducing oxidative stress in rats with SIMD.

This study has the following limitations. 1) In this study, an M12S transducer was used for STE, not a special small animal probe, but the chest wall of rats was thin with good resolution. The heart is smaller, heart rate is faster, and the boundaries of each section of the LV short axis are not obvious in rats compared with infants. Therefore, only LS was selected for segmental analysis. 2) For each rat, the images were obtained by a single sonographer using a single acquisition echocardiography machine. In the future, variability in rats from different acquisition devices, different cardiac cycles, or multiple sonographers should be evaluated. 3) In this study, we used two-dimensional and not three-dimensional echocardiography. Therefore, out-of-plane motion may have occurred, which may have affected measurements. However, we only selected images that were suitable for tracking.

In conclusion, this is the first study to show that naringin preserves heart function

in rats with SIMD by increasing cardiac antioxidant expression associated with the Keap1/Nrf2/HO-1 signaling pathway. Layer-specific strain analysis of myocardial function could reflect changes in myocardial systolic function at an early stage, providing an experimental basis for treating myocardial injury with naringin.

## Declaration of conflicting interest

The authors declare that there is no conflict of interest.

## Funding

This research received no specific grant from any funding agency in the public, commercial, or not-for-profit sectors.

## ORCID iD

Li-juan Sun https://orcid.org/0000-0003-1825-9195

## References

1. Wang HE, Jones AR and Donnelly JP. Revised National Estimates of Emergency Department Visits for Sepsis in the United States. *Crit Care Med* 2017; 45: 1443–1449. DOI: 10.1097/CCM.0000000000002538.
2. Singer M, Deutschman CS, Seymour CW, et al. The Third International Consensus Definitions for Sepsis and Septic Shock (Sepsis-3). *JAMA* 2016; 315: 801–810. DOI: 10.1001/jama.2016.0287.
3. Zhang N, Feng H, Liao HH, et al. Myricetin attenuated LPS induced cardiac injury in vivo and in vitro. *Phytother Res* 2018; 32: 459–470. DOI: 10.1002/ptr.5989.
4. Yao X, Carlson D, Sun Y, et al. Mitochondrial ROS Induces Cardiac Inflammation via a Pathway through mtDNA Damage in a Pneumonia-Related Sepsis Model. *PLoS One* 2015; 10: e0139416. DOI: 10.1371/journal.pone.0139416.
5. Drosatos K, Lymperopoulos A, Kennel PJ, et al. Pathophysiology of sepsis-related cardiac dysfunction: driven by inflammation, energy mismanagement, or both? *Curr Heart Fail Rep* 2015; 12: 130–140. DOI: 10.1007/s11897-014-0247-z.
6. Kawaguchi R, Hirata N, Tokinaga Y, et al. Nitrite administration improves sepsis-induced myocardial and mitochondrial dysfunction by modulating stress signal responses. *J Anesth* 2017; 31: 885–894. DOI: 10.1007/s00540-017-2417-0.
7. Immenschuh S, Baumgart-Vogt E and Mueller S. Heme oxygenase-1 and iron in liver inflammation: a complex alliance. *Curr Drug Targets* 2010; 11: 1541–1550. DOI: 10.2174/1389450111009011541.
8. Li X, Wu D and Tian Y. Fibroblast growth factor 19 protects the heart from oxidative stress-induced diabetic cardiomyopathy via activation of AMPK/Nrf2/HO-1 pathway. *Biochem Biophys Res Commun* 2018; 502: 62–68. DOI: 10.1016/j.bbrc.2018.05.121.
9. Yu H, Chen B and Ren Q. Baicalin relieves hypoxia-aroused H9c2 cell apoptosis by activating Nrf2/HO-1-mediated HIF1alpha/BNIP3 pathway. *Artif Cells Nanomed Biotechnol* 2019; 47: 3657–3663. DOI: 10.1080/21691401.2019.1657879.
10. Caglayan C, Temel Y, Kandemir FM, et al. Naringin protects against cyclophosphamide-induced hepatotoxicity and nephrotoxicity through modulation of oxidative stress, inflammation, apoptosis, autophagy, and DNA damage. *Environ Sci Pollut Res Int* 2018; 25: 20968–20984. DOI: 10.1007/s11356-018-2242-5.
11. Bharti S, Rani N, Krishnamurthy B, et al. Preclinical evidence for the pharmacological actions of naringin: a review. *Planta Med* 2014; 80: 437–451. DOI: 10.1055/s-0034-1368351.
12. Ivey KL, Hodgson JM, Croft KD, et al. Flavonoid intake and all-cause mortality. *Am J Clin Nutr* 2015; 101: 1012–1020. DOI: 10.3945/ajcn.113.073106.
13. Lim YJ, Kim JH, Pan JH, et al. Naringin Protects Pancreatic beta-Cells Against Oxidative Stress-Induced Apoptosis by Inhibiting Both Intrinsic and Extrinsic Pathways in Insulin-Deficient Diabetic Mice. *Mol Nutr Food Res* 2018; 62. DOI: 10.1002/mnfr.201700810.
14. Adil M, Kandhare AD, Ghosh P, et al. Sodium arsenite-induced myocardial bruise

in rats: Ameliorative effect of naringin via TGF-beta/Smad and Nrf/HO pathways. *Chem Biol Interact* 2016; 253: 66–77. DOI: 10.1016/j.cbi.2016.05.015.
15. Sun LJ, Qiao W, Xiao YJ, et al. Naringin mitigates myocardial strain and the inflammatory response in sepsis-induced myocardial dysfunction through regulation of PI3K/AKT/NF-kappaB pathway. *Int Immunopharmacol* 2019; 75: 105782. DOI: 10.1016/j.intimp.2019.105782.
16. Cong J, Wang Z, Jin H, et al. Quantitative evaluation of longitudinal strain in layer-specific myocardium during normal pregnancy in China. *Cardiovasc Ultrasound* 2016; 14: 45. DOI: 10.1186/s12947-016-0089-9.
17. Shiino K, Yamada A, Scalia GM, et al. Early Changes of Myocardial Function After Transcatheter Aortic Valve Implantation Using Multilayer Strain Speckle Tracking Echocardiography. *Am J Cardiol* 2019; 123: 956–960. DOI: 10.1016/j.amjcard.2018.12.008.
18. Bachner-Hinenzon N, Ertracht O, Malka A, et al. Layer-specific strain analysis: investigation of regional deformations in a rat model of acute versus chronic myocardial infarction. *Am J Physiol Heart Circ Physiol* 2012; 303: H549–H558. DOI: 10.1152/ajpheart.00294.2012.
19. Tavener SA, Long EM, Robbins SM, et al. Immune cell Toll-like receptor 4 is required for cardiac myocyte impairment during endotoxemia. *Circ Res* 2004; 95: 700–707. DOI: 10.1161/01.RES.0000144175.70140.8c.
20. Xianchu L, Lan PZ, Qiufang L, et al. Naringin protects against lipopolysaccharide-induced cardiac injury in mice. *Environ Toxicol Pharmacol* 2016; 48: 1–6. DOI: 10.1016/j.etap.2016.09.005.
21. Adebiyi OA, Adebiyi OO and Owira PM. Naringin Reduces Hyperglycemia-Induced Cardiac Fibrosis by Relieving Oxidative Stress. *PLoS One* 2016; 11: e0149890. DOI: 10.1371/journal.pone.0149890.
22. He H, Chang X, Gao J, et al. Salidroside Mitigates Sepsis-Induced Myocarditis in Rats by Regulating IGF-1/PI3K/Akt/GSK-3beta Signaling. *Inflammation* 2015; 38: 2178–2184. DOI: 10.1007/s10753-015-0200-7.
23. Viswanatha GL, Shylaja H and Moolemath Y. The beneficial role of Naringin- a citrus bioflavonoid, against oxidative stress-induced neurobehavioral disorders and cognitive dysfunction in rodents: A systematic review and meta-analysis. *Biomed Pharmacother* 2017; 94: 909–929. DOI: 10.1016/j.biopha.2017.07.072.
24. Chu M, Gao Y, Zhou B, et al. Circumferential Strain Can Be Used to Detect Lipopolysaccharide-Induced Myocardial Dysfunction and Predict the Mortality of Severe Sepsis in Mice. *PLoS One* 2016; 11: e0155346. DOI: 10.1371/journal.pone.0155346.
25. Cong J, Lee Y, Fu X, et al. Quantitative evaluation of longitudinal strain in layer-specific myocardium in patients with pre-eclampsia. *Int J Cardiovasc Imaging* 2018; 34: 193–200. DOI: 10.1007/s10554-017-1220-1.
26. Suzuki R, Mochizuki Y, Yoshimatsu H, et al. Layer-specific myocardial function in asymptomatic cats with obstructive hypertrophic cardiomyopathy assessed using 2-dimensional speckle-tracking echocardiography. *J Vet Intern Med* 2019; 33: 37–45. DOI: 10.1111/jvim.15339.
27. Nagata Y, Wu VC, Otsuji Y, et al. Normal range of myocardial layer-specific strain using two-dimensional speckle tracking echocardiography. *PLoS One* 2017; 12: e0180584. DOI: 10.1371/journal.pone.0180584.
28. Sarvari SI, Haugaa KH, Zahid W, et al. Layer-specific quantification of myocardial deformation by strain echocardiography may reveal significant CAD in patients with non-ST-segment elevation acute coronary syndrome. *JACC Cardiovasc Imaging* 2013; 6: 535–544. DOI: 10.1016/j.jcmg.2013.01.009.
29. Senoner T and Dichtl W. Oxidative Stress in Cardiovascular Diseases: Still a Therapeutic Target? *Nutrients* 2019; 11: 2090. DOI: 10.3390/nu11092090.
30. Mantzarlis K, Tsolaki V and Zakynthinos E. Role of Oxidative Stress and Mitochondrial Dysfunction in Sepsis and Potential

Therapies. *Oxid Med Cell Longev* 2017; 2017: 5985209. DOI: 10.1155/2017/5985209.
31. Xu J, Lin C, Wang T, et al. Ergosterol Attenuates LPS-Induced Myocardial Injury by Modulating Oxidative Stress and Apoptosis in Rats. *Cell Physiol Biochem* 2018; 48: 583–592. DOI: 10.1159/000491887.
32. Requena JR, Fu MX, Ahmed MU, et al. Lipoxidation products as biomarkers of oxidative damage to proteins during lipid peroxidation reactions. *Nephrol Dial Transplant* 1996; 11: 48–53. DOI: 10.1093/ndt/11.supp5.48.
33. Yang M, Xiong J, Zou Q, et al. Chrysin attenuates interstitial fibrosis and improves cardiac function in a rat model of acute myocardial infarction. *J Mol Histol* 2018; 49: 555–565. DOI: 10.1007/s10735-018-9793-0.
34. Liu S, Zhang X and Wang J. Isovitexin protects against cisplatin-induced kidney injury in mice through inhibiting inflammatory and oxidative responses. *Int Immunopharmacol* 2020; 83: 106437. DOI: 10.1016/j.intimp.2020.106437.
35. Chen QY, Wang GG, Li W, et al. Heme Oxygenase-1 Promotes Delayed Wound Healing in Diabetic Rats. *J Diabetes Res* 2016; 2016: 9726503. DOI: 10.1155/2016/9726503.
36. Mo M, Li S, Dong Z, et al. S-allylmercaptocysteine ameliorates lipopolysaccharide-induced acute lung injury in mice by inhibiting inflammation and oxidative stress via nuclear factor kappa B and Keap1/Nrf2 pathways. *Int Immunopharmacol* 2020; 81: 106273. DOI: 10.1016/j.intimp.2020.106273.